Global Compartmental Analysis of the Excited-State Reaction between Fluorescein and (±)-*N*-Acetyl Aspartic Acid

Luis Crovetto, Angel Orte, Eva M. Talavera, and Jose M. Alvarez-Pez*

Department of Physical Chemistry, University of Granada, Cartuja Campus, Granada 18071, Spain

Mircea Cotlet, Jan Thielemans, Frans C. De Schryver, and Noël Boens

Department of Chemistry, Katholieke Universiteit Leuven, Celestijnenlaan 200 F, 3001 Heverlee, Belgium

Received: December 4, 2003; In Final Form: February 11, 2004

Fluorescein is a complex fluorophore which at the physiological pH can exist as mono- and dianion forms. In a previous article (*J. Phys. Chem. A* **2001**, *105*, 6320−6332), we showed that fluorescein displays an excited-state proton transfer reaction which interconverts the mono- and dianion forms in the presence of a suitable proton donor−acceptor. Because fluorescein is a frequently used fluorescent label in biological systems, it is of interest to know if amino acids with acidic side chains are able to induce fluorescein excited-state proton transfer reactions. We have selected (±)-*N*-acetyl aspartic acid, *N*-AcAsp, as a model donor−acceptor which mimics the interaction of the aspartic acid residues with the fluorescent label in native proteins. We present absorption and emission properties which show that *N*-AcAsp at 1 M concentration induces the excited-state proton transfer reaction between the mono- and dianion of fluorescein. The kinetics of this excited-state process was characterized from time-resolved fluorescence measurements, and the analysis was done within the framework of global compartmental analysis. Thus, we have formulated the fluorescence decay analysis of intermolecular two-state excited-state processes in the presence of buffer in terms of compartments. The kinetic equations describing the excited-state species concentrations were derived, and the expressions for the fluorescence decay surface were obtained. The experimental fluorescence decay data surface of fluorescein in the presence of 1 M *N*-AcAsp concentration at different pH values and excitation and emission wavelengths was analyzed via this new global compartmental analysis method, to recover the rate constants and the spectral parameters related to absorption and emission of the excited-state proton transfer reaction.

Introduction

Fluorescein is a complex molecule which, in aqueous solution, can exist in one or more of four different prototropic forms (cation, neutral, monoanion, and dianion) depending on pH.[1] The ground-state pK_a values for the different equilibria are as follows: cation−neutral pK_C = 2.19, neutral−monoanion pK_N = 4.4, monoanion−dianion pK_M = 6.36.[2] Therefore, in the physiological pH range only the dianion and monoanion forms are important. Their chemical structures and ground-state proton reaction are shown in Figure 1. In previous articles we have shown that in the presence of 1 M phosphate buffer, which acts as a suitable proton donor−acceptor, the excited-state monoanion−dianion proton transfer reaction occurs very efficiently and the fluorescence decays of the excited monoanion and dianion become coupled. However, at low buffer concentrations (5 mM phosphate buffer or less) and in the pH range of 6 to 10, the excited monoanion and dianion are not coupled by the excited-state proton reaction and thus decay independently of each other.[3,4]

Because fluorescein is commonly used as a fluorescent label in biological systems, such as proteins, in which a proton donor−acceptor other than phosphate buffer may be present, it is of interest to know if amino acids with acidic side chains are able to induce fluorescein excited-state proton exchange reactions. We have selected (±)-*N*-acetyl aspartic acid, *N*-AcAsp, as a donor−acceptor with proton transfer properties, (pK_{a1} = 3.09 and pK_{a2} = 4.52)[5] relatively similar to those of fluorescein monoanion−dianion pK_a^* (6.41). Moreover, as is known, the environment around the ionizable group in an ordered structure such as a native protein will greatly influence the pK_a of the acidic side chain. Aspartic acid can be considered as an extreme example of these changes in the apparent pK_a and there are thus aspartic residues having pK_a > 9[6] and others having pK_a ≤ 1.[7,8] In order to understand the more complex behavior of fluorescein-labeled proteins influenced by the acidic side chain of aspartic

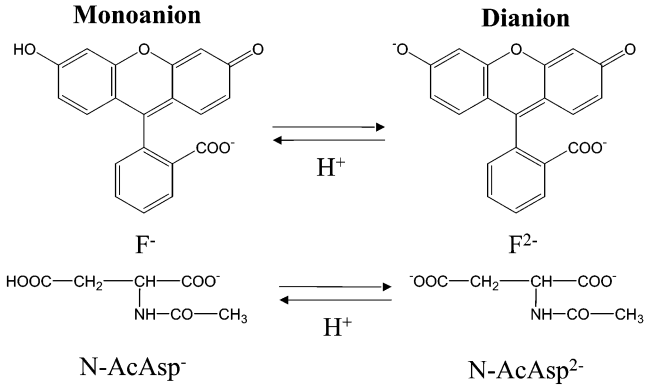

Figure 1. Chemical structures and ground-state proton exchange reactions of fluorescein and *N*-AcAsp mono- and dianion.

* To whom correspondence should be addressed. Phone: + 34-958-243831. Fax: + 34-958-244090. E-mail: jalvarez@ugr.es.

10.1021/jp0313019 CCC: $27.50
Published on Web 04/17/2004

acid, we choose the fluorescein−*N*-AcAsp model system which mimics the interaction of the aspartic acid residues with the fluorescent label in native proteins.

The time-resolved fluorescence study of the fluorescein monoanion−dianion proton exchange reaction is a challenging problem because of the strong overlap of the absorption[1] and emission[9] spectra of the mono- and dianion and because the pK_a values of the monoanion−dianion reaction in the excited and ground states are very similar.[3,4] Moreover, because of the *N*-AcAsp pK_a values (3.09 and 4.52),[5] the upper pH value of interest to resolve this monoanion−dianion equilibrium is limited to pH 7. Consequently, the experimental data can only be obtained in the pH range of around 6. Because of this complexity, a powerful method of analysis is needed to extract the relevant kinetic and spectral parameters from the experimental data.

The kinetics of excited-state processes can be characterized from time-resolved measurements of the concomitant fluorescence. The single-photon timing (SPT) methodology provides fluorescence decay data with high enough accuracy to allow an elaborate data analysis.

In many cases the time relaxation of an excited-state system can be described by a sum of exponential functions in terms of decay times and the corresponding preexponential factors. However, these descriptive parameters are not of prime interest, but rather the rate constants defining the excited states and the species-associated excitation and emission spectra are the important parameters. To determine these more fundamental parameters, a multidimensional fluorescence decay data surface is measured under a variety of experimental conditions. From the resulting set of decay times and preexponential factors, the rate constants and the species-associated spectra can then be derived. An accurate determination of the decay times and the preexponentials can be obtained by the global analysis approach where parameters can be linked over various decay curves (e.g., the decay times can be linked over decay traces collected at various emission wavelengths).[10−12] However, for decay traces collected at various concentrations of a coreactant the decay times generally vary and hence cannot be linked. To benefit the most from the merits of a global analysis approach, one has to fit directly for the underlying parameters, that is, the rate constants which can indeed be linked. This global compartmental analysis has the additional advantage that the parameters of interest are determined directly from the complete decay data surface in a single step.[13−16]

Compartmental models are extensively used in many branches of the biosciences and engineering.[17−19] The modeling of excited-state processes can also conveniently be done within the framework of compartmental analysis. However, its use in photophysics is of recent date.[13−16, 20−25]

In a photophysical framework a compartment is a subsystem composed of a distinct type of species that acts kinetically in a unique way. The concentration of the constituting species can change when the compartments exchange material through intermolecular (or intramolecular) processes. Compartments can be divided into ground and excited-state compartments depending upon the state of the composing species. There may be inputs from the ground-state compartments into one or more of the excited-state compartments by light excitation. There is always output from the excited-state compartments to the ground-state compartments through deactivation processes such as fluorescence, internal conversion, and intersystem crossing. If the concentrations of the species in the ground state do not significantly change upon excitation, it suffices to consider the excited-state compartments only (the ground-state compartments can then be lumped together as the external environment). Compartments are generally depicted as boxes (see Scheme 1), circles, or ovals which enclose the composing species. Single-headed arrows pointing away from a compartment are used to represent outflow from that compartment, whereas single-headed arrows pointing toward a compartment depict inflow into that compartment.

SCHEME 1: Kinetic Model of Ground and Excited-State Proton Exchange Reactions[a]

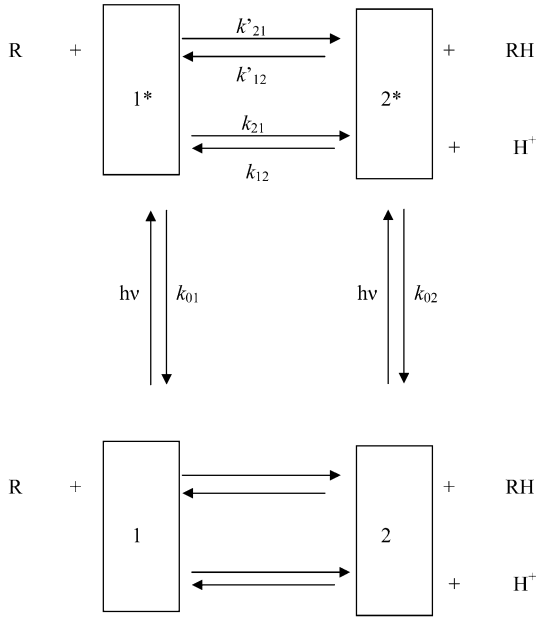

[a] 1 and 2 are the ground-state conjugate acid base forms of the fluorophore, whereas 1* and 2* are the corresponding excited species.

In this paper we shall formulate the fluorescence decay analysis of intermolecular two-state excited-state processes with added buffer in terms of compartments (see Scheme 1). First, the kinetic equations describing the excited-state species concentrations will be derived and expressions for the fluorescence decay surface will be given. Second, the experimental fluorescence decay data surface of the fluorescein mono- and dianion in the presence of *N*-AcAsp under different experimental conditions will be analyzed via this new global compartmental analysis method to recover the relevant rate constants of the excited-state proton transfer reaction between these two ionic forms and the spectral parameters related to absorption and emission.

Kinetics

Consider a dynamic, linear, time-invariant, intermolecular system consisting of two distinct types of ground-state species and two corresponding excited-state species as depicted in Scheme 1 (i.e., two ground-state compartments and two associated excited-state compartments). Excitation by light creates the excited-state species 1* and 2*, which can decay by fluorescence (F) and nonradiative (NR) processes. The composite rate constant for these processes is denoted by k_{0i} ($= k_{Fi} + k_{NRi}$) for species i*. k_{21} represents the first-order rate constant for the dissociation of 1* into 2* and H^+, whereas k_{12} is the second-order rate constant for association of 2* and H^+ to form 1*. k'_{21} is the second-order rate constant for the reaction 1* + R → 2* + RH, whereas k'_{12} denotes the second-order rate constant for the reverse reaction 2* + RH → 1* + R. All rate constants k_{ij}

are non-negative. R and RH represent, respectively, the base and conjugate acid form of the buffer.

If the system shown in Scheme 1 is excited with a δ-pulse at time $t = 0$ which does not significantly change the concentrations of the ground-state species, the time course of the concentrations of the excited-state species 1* and 2* is described by the first-order differential equation

$$\dot{\boldsymbol{x}}(t) = \boldsymbol{A}\boldsymbol{x}(t), \quad t \geq 0 \tag{1}$$

$\boldsymbol{x}(t)$ is the 2×1 vector function of the concentrations of the excited-state species 1* and 2*:

$$\begin{bmatrix} x_1(t) \\ x_2(t) \end{bmatrix} = \begin{bmatrix} [1^*](t) \\ [2^*](t) \end{bmatrix} \tag{2}$$

$\dot{\boldsymbol{x}}(t)$ denotes its time derivative and $\boldsymbol{A}$ is the 2×2 compartmental matrix

$$\boldsymbol{A} = \begin{bmatrix} -(k_{01} + k_{21} + k'_{21}[\mathrm{R}]) & k_{12}[\mathrm{H^+}] + k'_{12}[\mathrm{RH}] \\ k_{21} + k'_{21}[\mathrm{R}] & -(k_{02} + k_{12}[\mathrm{H^+}] + k'_{12}[\mathrm{RH}]) \end{bmatrix} \tag{3}$$

with the concentrations of species i^* at time zero defined by $\boldsymbol{x}(0) = \boldsymbol{b}$ where $\boldsymbol{b}$ is the 2×1 column vector with elements b_i ($i = 1, 2$). $\boldsymbol{b}$ depends on the excitation wavelength λ^{ex} and the concentrations [R], [RH], and [H^+]. The solution of the system of differential equations (eq 1) is given by

$$\boldsymbol{x}(t) = \mathrm{e}^{\boldsymbol{A}t}\boldsymbol{b}, \quad t \geq 0 \tag{4}$$

If we assume that the 2×2 compartmental matrix $\boldsymbol{A}$ has two linearly independent eigenvectors $\boldsymbol{U}_1$ and $\boldsymbol{U}_2$ associated with the eigenvalues γ_1 and γ_2, respectively, that is, $\boldsymbol{A} = \mathbf{U}\Gamma\mathbf{U}^{-1}$ with $\mathbf{U} = [\boldsymbol{U}_1, \boldsymbol{U}_2]$ and $\mathbf{U}^{-1}$ the inverse of the matrix of the eigenvectors, and $\Gamma = \mathrm{diag}\ (\gamma_1, \gamma_2)$, eq 4 can then be rewritten as

$$\boldsymbol{x}(t) = \mathbf{U}\mathrm{e}^{\Gamma t}\mathbf{U}^{-1}\boldsymbol{b}, \quad t \geq 0 \tag{5}$$

where $\exp(\Gamma t) = \mathrm{diag}\ [\exp(\gamma_1 t), \exp(\gamma_2 t)]$. $\mathbf{U}$ and $\exp(\Gamma t)$ are functions of the rate constants k_{ij} and the concentrations [R], [RH], and [H^+]. The impulse response function, $f(\lambda^{ex},\lambda^{em},t)$, at emission wavelength λ^{em} due to excitation at λ^{ex} is given by[15]

$$f(\lambda^{ex},\lambda^{em},t) = \boldsymbol{c}(\lambda^{em})\boldsymbol{x}(t) = \boldsymbol{c}(\lambda^{em})\,\mathrm{e}^{\boldsymbol{A}t}\boldsymbol{b}, \quad t \geq 0 \tag{6}$$

The dependence of $f(t)$ on λ^{ex} arises from the λ^{ex} dependence of $\boldsymbol{b}$. $\boldsymbol{c}(\lambda^{em})$ is the 1×2 vector of the emission weighting factors $c_i(\lambda^{em})$ of species i^* at λ^{em}. $c_i(\lambda^{em})$ is given by[15]

$$c_i(\lambda^{em}) = k_{Fi}\int_{\Delta\lambda^{em}} \rho_i(\lambda^{em})\,\mathrm{d}\lambda^{em} \tag{7}$$

k_{Fi} is the fluorescence rate constant of i^*; $\Delta\lambda^{em}$ is the emission wavelength interval around λ^{em} where the fluorescence signal is monitored; $\rho_i(\lambda^{em})$ is the emission density of i^* at λ^{em} defined by[15]

$$\rho_i(\lambda^{em}) = \mathrm{F}_i(\lambda^{em},\lambda^{ex}) / \int_{\text{full emission band}} \mathrm{F}_i(\lambda^{em},\lambda^{ex})\,\mathrm{d}\lambda^{em} \tag{8}$$

where the integration extends over the whole steady-state fluorescence spectrum F_i of species i^*.

Equation 6 can be written in the common biexponential format:

$$f(t) = \alpha_1\,\mathrm{e}^{\gamma_1 t} + \alpha_2\,\mathrm{e}^{\gamma_2 t}, \quad t \geq 0 \tag{9}$$

The eigenvalues γ_i ($i = 1, 2$) of the compartmental matrix $\boldsymbol{A}$ are related to the decay times τ_i ($i = 1, 2$) according to

$$\gamma_i = -1/\tau_i \tag{10}$$

and are given by

$$\gamma_i = -\frac{1}{2}\{a_{11} - a_{22} \mp [(a_{22} - a_{11})^2 + 4a_{12}a_{21}]^{1/2}\} \tag{11}$$

with a_{ij} the ijth element of the compartmental matrix $\boldsymbol{A}$ (eq 3).

If the elements b_i of $\boldsymbol{b}$ are normalized as

$$\tilde{b}_i = b_i / \sum_{j=1}^{2} b_j, \quad i = 1, 2 \tag{12}$$

and similarly the elements c_i of $\boldsymbol{c}$ as

$$\tilde{c}_i = c_i / \sum_{j=1}^{2} c_j, \quad i = 1, 2 \tag{13}$$

eq 6 can be written as

$$f(\lambda^{ex}, \lambda^{em}, t) = \kappa\tilde{\boldsymbol{c}}(\lambda^{em})\,\mathrm{e}^{\boldsymbol{A}t}\tilde{\boldsymbol{b}}, \quad t \geq 0 \tag{14}$$

with κ a proportionality constant. The use of κ, $\tilde{b}_i$, and $\tilde{c}_i$ allows one to link $\tilde{b}_i$ and $\tilde{c}_i$ in the data analysis so that the collected decay traces are not required to be scaled. Indeed, $\tilde{\boldsymbol{b}}$ depends on λ^{ex} and the concentrations [R], [RH], and [H^+], whereas $\tilde{\boldsymbol{c}}(\lambda^{em})$ depends on the emission wavelength only. In our implementation of global compartmental analysis one fits directly for the rate constants k_{01}, k_{21}, k_{02}, (k_{12}), k'_{12}, k'_{21}, the normalized zero-time concentrations $\tilde{b}_1$ of species 1*, and the normalized spectral emission weighting factors $\tilde{c}_1(\lambda^{em})$ of species 1*.

If the compartmental matrix $\boldsymbol{A}$ has two distinct eigenvalues γ_1 and γ_2 with corresponding eigenvectors $\boldsymbol{U}_1$ and $\boldsymbol{U}_2$, respectively, eq 14 can be formulated as

$$f(\lambda^{ex}, \lambda^{em}, t) = \kappa\tilde{\boldsymbol{c}}(\lambda^{em})\mathbf{U}\mathrm{e}^{\Gamma t}\mathbf{U}^{-1}\tilde{\boldsymbol{b}}, \quad t \geq 0 \tag{15}$$

Materials and Methods

Reagents. Sodium hydroxide and ethanol were from Merck. Fluorescein acid yellow (free acid crystalline) and *N*-AcAsp were from Sigma Chemical Co. Fluorescein was purified by recrystallization from ethanol. The purified product was checked by means of fluorescence and absorption spectra as well as by thin-layer chromatography. All other chemicals were used without further purification.

Solutions. Fluorescein solutions were prepared by dissolving fluorescein in 1 mL of deionized−distilled water containing 0.1 mL of 1 M NaOH. The volume of the latter solution was increased to 50 mL by the addition of water to give a 5×10^{-4} M fluorescein solution. 2.5×10^{-5} M fluorescein solutions with appropriate *N*-AcAsp concentration were prepared by dissolving *N*-AcAsp in deionized−distilled water and adding 0.25 mL of 5×10^{-4} M fluorescein solution and 1 M NaOH to obtain different pH values and 5 mL of volume. For high pH solutions, the pH was adjusted with NaOH. Fluorescein solutions were

TABLE 1: Values for the Rate Constants k_{ij} and the Spectral Parameters $\tilde{b}_1$ and $\tilde{c}_1$ Estimated by Global Compartmental Analysis, According to Scheme 2, of the Experimental Fluorescence Decay Surface of Fluorescein Measured in the Presence of 1 M *N*-AcAsp as a Function of pH, λ^{em}, and λ^{ex}

k_{ij}	
$k_{01} + k_{21}$ (ns^{-1})	0.2765 (± 0.004)
k_{02} (ns^{-1})	0.231[a]
k_{12} (M^{-1} ns^{-1})	0[a]
k'_{12} (M^{-1} ns^{-1})	0.012 (± 0.0015)
k'_{21} (M^{-1} ns^{-1})	0.0336 (±0.0015)

pH	λ^{ex} (nm)	$\tilde{b}_1$
6.02	420	0.922 (± 0.002)
6.02	440	0.883 (± 0.002)
6.20	420	0.832 (± 0.002)
6.20	440	0.827 (± 0.002)
6.40	420	0.822 (± 0.002)
6.40	440	0.817 (± 0.002)
6.58	420	0.778 (± 0.002)

λ^{em} (nm)	$\tilde{c}_1(\lambda^{em})$
580	0.481 (± 0.002)
550	0.402 (± 0.002)
530	0.298 (± 0.002)
515	0.260 (± 0.002)

[a] Kept constant during the fitting procedure.

kept cool in the dark when not in use to avoid deterioration by exposure to light[2] and heat.[26]

Steady-State Measurements. Absorption spectra were recorded with a GBC Cintra 10e UV−vis spectrophotometer with a temperature-controlled cell holder using 1 cm light path cuvettes. Steady-state fluorescence spectra were recorded on a Perkin-Elmer LS 55 spectrofluorometer operating in the L format with a temperature-controlled cell holder using 1 cm light path cuvettes. All measurements were done at room temperature.

Laser System for SPT Measurements. A laser-based excitation-wavelength-tunable system with SPT detection was used to record fluorescence decay traces. It allows convenient selection of excitation wavelengths from 240 to 660 nm, with a gap between 335 and 360 nm. It consists of a mode-locked Ti:sapphire laser, pumped by all visible lines of a continuous wave Ar^+ laser, an optical parametric oscillator, pulse pickers, and second- and third-harmonics generators, delivering pulses with a fwhm of 1−2 ps. To detect the emission, a double monochromator and a microchannel plate are used. The classical SPT detection, comprising a trigger photodiode, signal amplifiers, optional delay line, a SPT PC module with two constant fraction discriminators, a time-to-amplitude converter and an analog-to-digital converter on board, is used. Full details of the picosecond laser system with SPT detection, including the brand names of all used optical, mechanical, and electronic components, and its performance characteristics have been reported elsewhere.[27]

Time-Resolved Fluorescence. Aqueous undegassed solutions containing 2.5×10^{-5} M of fluorescein and 1 M of *N*-AcAsp at pH 6.02, 6.20, 6.40, and 6.58 were used for the time-resolved emission measurements. All experiments were done at room temperature. Fluorescence decay traces were collected with the experimental setup described in the previous paragraph. Two excitation wavelengths (420 and 440 nm) were used, except at pH 6.58, in which only 420 nm excitation wavelength was used. The laser pulses were passed through a Berek compensator and a Glan−Thomson polarizer in order to obtain vertically polarized excitation light at the sample. Fluorescence was collected in

SCHEME 2: Kinetic Model of Ground and Excited-State Proton Transfer Reactions[a]

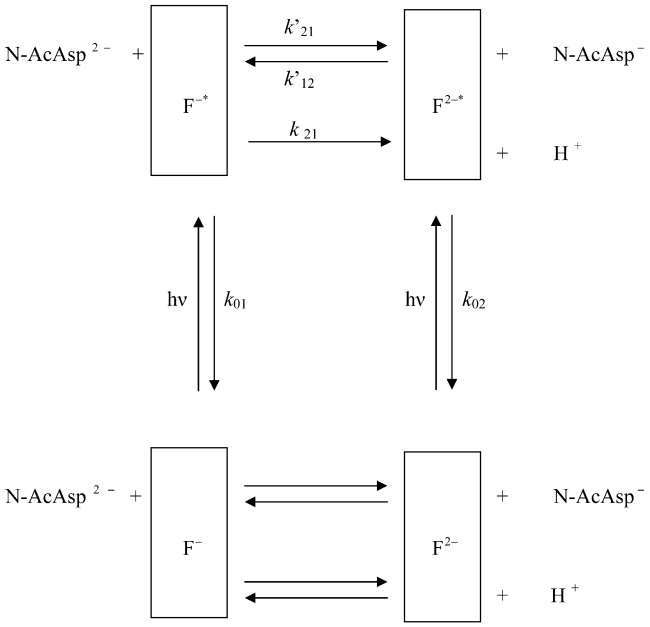

[a] F^- and F^{2-} are, respectively, the monoanion and dianion of fluorescein (see Figure 1). F^{-*} and F^{2-*} are the corresponding excited-state species. *N*-$AcAsp^{2-}$ and *N*-$AcAsp^-$ are the dianionic and monoanionic forms of *N*-AcAsp, respectively (see Figure 1).

right angle geometry after passing through a collimating lens and a polarizer set at the magic angle (54.7°) with respect to the excitation polarization. The selection of the emission wavelengths (480, 500, 515, 530, 550, and 580 nm) was done with a stepper-motor-controlled double monochromator with 5 nm resolution. Finally the fluorescence was detected with a cooled microchannel plate photomultiplier. The experimental instrument response function for the used excitation/emission wavelengths was in the 40−80 ps range. The entire decay data surface as a function of pH, excitation, and emission wavelengths contained 42 curves. All decay curves were collected in 4096 channels (6.95 ps/channel) with about 10 000 detected counts at the maximum. Each individual fluorescence decay trace was first analyzed as a biexponential (eq 9). Then all decays at the same pH were analyzed globally as biexponential functions (eq 9) in terms of preexponentials α and lifetimes τ with the lifetimes linked. Finally 28 decays, at different pH, λ^{ex}, and λ^{em} (see Table 1), were selected to be analyzed according to the global compartmental model discussed in the text (Scheme 2). For the experimental fluorescein−*N*-AcAsp system the general kinetic model shown in Scheme 1 was substituted by that in Scheme 2. Here 1 and 2 represent, respectively, the monoanion (F^-) and dianion (F^{2-}) forms of fluorescein (see Figure 1 for their chemical structures). *N*-$AcAsp^-$ and *N*-$AcAsp^{2-}$ are, respectively, the monoanion and dianion forms of *N*-AcAsp (see Figure 1 for their chemical structures). F^{-*} and F^{2-*} are the associated excited states of the monoanion and dianion, respectively, of fluorescein. $\tilde{b}_1(\lambda^{ex}, \text{pH})$ is the normalized zero-time concentration of F^{-*} at the specified λ^{ex} and pH. $\tilde{c}_1(\lambda^{em})$ corresponds to the emission weighting factor of F^{-*} at λ^{ex}. The parameters were linked as shown in Scheme 3. Because of the low value of $[H^+]$ in the pH range used, the contribution of $k_{12}[H^+]$ to $\boldsymbol{A}$ (eq 3) and the lifetimes is negligible. Indeed, the lifetimes of fluorescein in the absence of buffer are invariant in the pH region studied. Therefore, the proton transfer reaction toward F^{2-*} to form F^{-*} can be

SCHEME 3: Linking Scheme for the Global Compartmental Analysis (Scheme 1) of Decays Recorded at *i* Emission Wavelengths λ^{em} Due to Two Excitation Wavelengths λ^{ex} [a]

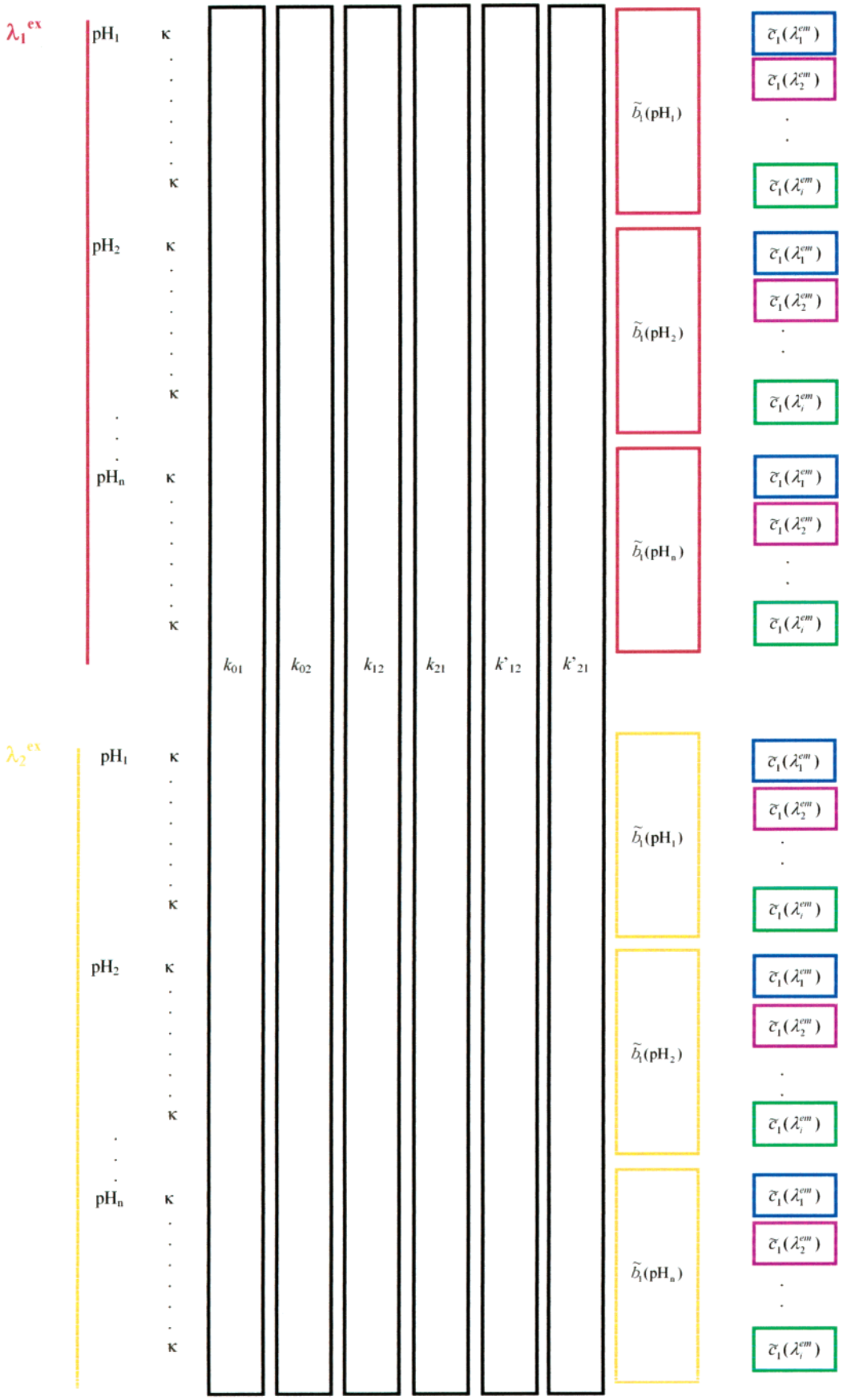

[a] Boxed parameters in the same color indicate linked parameters, whereas κ denotes the local scaling factors. The rate constants k_{ij} are linked over the entire fluorescence decay surface; $\tilde{b}_1$ is linked at the same λ^{ex} and pH; $\tilde{c}_1$ is linked at the same λ^{em}.

neglected by setting $k_{12} = 0$ during the curve fitting. The rate constants k_{ij} are independent of λ^{ex}, λ^{em}, and pH, and hence can be linked over the entire fluorescence decay data surface. The emission weighting factors $\tilde{c}_1$ (λ^{em}) only depend on λ^{em}, and therefore can be linked at the same emission wavelength. The spectral parameters $\tilde{b}_1(\lambda^{ex}, \text{pH})$ are dependent on both λ^{ex} and pH and consequently can only be linked at the same λ^{ex} and pH.

Because the fluorescence decay data surface was collected as a function of pH at a single buffer concentration (1 M *N*-AcAsp), it is crucial to know what information about the rate constants and spectral parameters can be extracted from such a global fluorescence decay surface. The deterministic identifiability analysis (to be published separately) shows that if the only known information about the rate constants is the value of k_{02}, the four other rate constants (k_{01}, k_{21}, k'_{21}, and k'_{12}) cannot be determined from decay traces measured as a function of pH at a common buffer concentration. However, if both k_{01} and k_{02} are known, the remaining rate constants (k_{21}, k'_{21}, and k'_{12}) can be uniquely determined from decay traces collected at a common buffer concentration as a function of pH. The nonnegativity requirement of $\tilde{b}_1(\lambda^{ex}, \text{pH})$ and $\tilde{c}_1(\lambda^{em})$, together with the upper limit of one, implemented in the global compartmental analysis program, also is helpful in obtaining unique parameter estimates. Moreover, the dependence of $\tilde{b}_1(\lambda^{ex}, \text{pH})$ on pH puts additional constraints on this parameter. The results of the deterministic identifiability analysis require that k_{01} and k_{02} be kept fixed during the global compartmental analyses to obtain unique parameters estimates. The values of k_{02} and the sum ($k_{01} + k_{21}$) are known from a biexponential decay of fluorescein in the absence of buffer. A unique value can be assigned to k_{02} from a monoexponential decay at high pH with $\tau = 1/k_{02}$. Hence, a series of global compartmental analyses was performed in which the value of k_{02} was kept fixed at its true value while k_{01} was held constant at various values ranging from zero to the sum ($k_{01} + k_{21}$).

Implementation of Global Compartmental Analysis. The global compartmental analysis of the fluorescence decay surface of species undergoing excited-state processes in the presence of added buffer was implemented in a general global analysis program using Gaussian-weighted nonlinear least-squares fitting based on Marquardt−Levenberg minimization.[28] Any of the fitting parameters can be kept fixed during the fitting or may be freely adjustable to seek optimum values.

Consider the intermolecular two-state excited-state process in the presence of added buffer as shown in Scheme 2. The global fitting parameters are k_{01}, k_{21}, k_{02}, $k_{12} = 0$, k'_{12}, k'_{21}, $\tilde{b}_1$, and $\tilde{c}_1(\lambda^{em})$. The only local fitting parameters are the scaling factors κ. [R] and [RH] are related to the total (analytical) buffer concentration, $C_B = [R] + [RH]$, its acidity constant K_a, and the pH of the buffer solution by the expressions $[R] = C_B K_a/(K_a + [H^+])$ and $[RH] = C_B[H^+]/(K_a + [H^+])$. For a certain buffer at a fixed total concentration, [R] and [RH] only depend on pH. Assigning initial guesses to the rate constants k_{01}, k_{21}, k_{02}, $k_{12} = 0$, k'_{12}, k'_{21} allows one to construct the compartmental matrix $\boldsymbol{A}$ for each decay trace. The eigenvalues γ and the associated eigenvectors of this matrix are determined using routines from EISPACK, matrix eigensystem routines.[29] The eigenvectors are then scaled to the initial conditions $\tilde{\boldsymbol{b}}$. The fluorescence δ-response of the sample, $f(\lambda^{ex}, \lambda^{em}, t)$ is calculated according eq 15. Then $f(\lambda^{ex}, \lambda^{em}, t)$ is convoluted with the experimental instrument response function, and the adjustable parameters of this calculated curve are optimized to fit the experimental fluorescence decay of the sample. When this approach is used, experiments done at different excitation/emission wavelengths, at multiple timing calibrations, and at different pH values are linked by all rate constants defining the system.

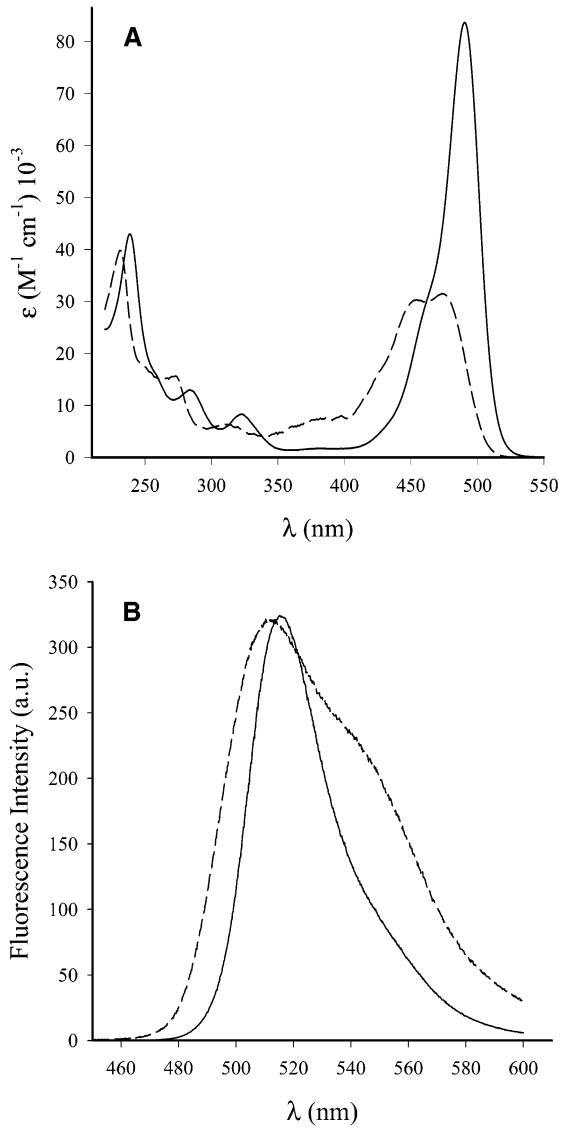

Figure 2. Absorption (A) and emission (B) spectra of fluorescein monoanion (− − −) and dianion (——). The extinction coefficient vs wavelength graphs were obtained by methods described in our previous publication.[3] To measure the emission spectra of the dianion and monoanion, we recorded fluorescence spectra at pH 11 ($\lambda^{ex} = 490$ nm) and pH 5.0 ($\lambda^{ex} = 440$ nm). These spectra correspond respectively to the dianion and monoanion. The monoanion spectrum was multiplied by a factor of 3 to show its fundamental characteristics.

The fitting parameters were determined by minimizing the *global reduced* chi-square χ_g^2

$$\chi_g^2 = \sum_{l}^{q} \sum_{i} w_{li}(y^o_{li} - y^c_{li})/\nu \qquad (16)$$

where the index l sums over q experiments and the index i sums over the appropriate channel limits for each individual experiment. y^o_{li} and y^c_{li} denote, respectively, the observed (experimentally measured) and calculated (fitted) values corresponding to the ith channel of the lth experiment, and w_{li} is the corresponding statistical weight. ν represents the number of degrees of freedom for the entire multidimensional fluorescence decay surface.

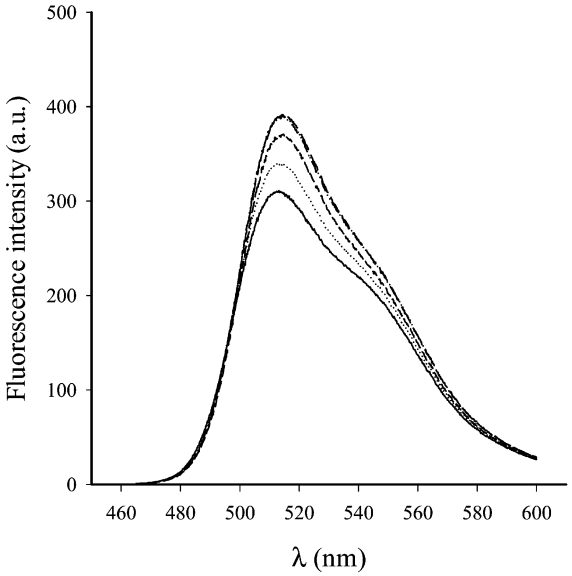

Figure 3. Steady-state fluorescence spectra of fluorescein (at $\lambda^{ex} =$ 440 nm, pH 5.9) showing an increase in intensity with increasing *N*-AcAsp concentration. The fluorescein concentration was 2.5×10^{-5} M, and *N*-AcAsp concentrations were 0, 0.1, 0.25, 0.5, and 1 M.

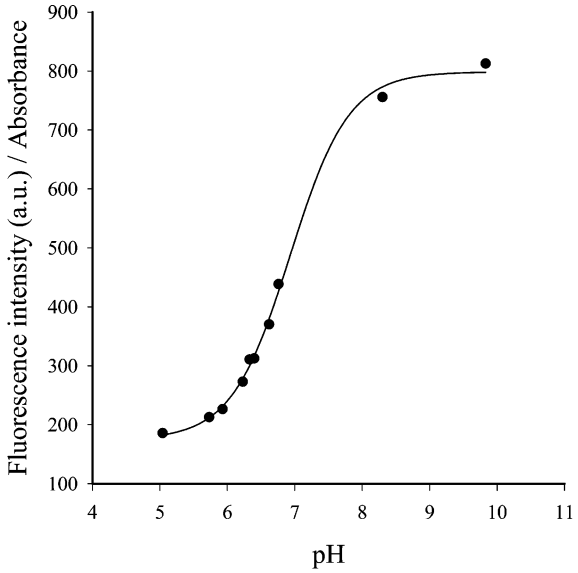

Figure 4. Plot of the experimental steady-state fluorescence intensity normalized by absorbance ($\lambda^{ex} = 440$ nm, $\lambda^{em} = 515$ nm) vs pH, from solutions of 2.5×10^{-5} M fluorescein and 1 M *N*-AcAsp. Equation 17 was fitted to these experimental values. The solid line represents the best fitting curve.

The statistical criteria to judge the quality of the fit comprised both graphical and numerical tests. The graphical methods included plots of surfaces ("carpets") of the autocorrelation function values versus experiment number and of the weighted residuals versus channel number versus experiment number.

Results and Discussion

It is known that the only significant forms of fluorescein in aqueous solution in the pH range of 5.5−11 are the monoanion and dianion ($pK_M = 6.36$).[30] Now we shall demonstrate the occurrence of the excited-state proton exchange reaction between fluorescein mono- and dianion if *N*-AcAsp is present at sufficiently high concentration (1 M). Likewise, we show that this reaction does not take place in the absence or at low concentration (less than or equal to 5 mM) of the proton donor−acceptor.

Absorption Spectra. The absorption and emission spectra of the fluorescein monoanion and dianion are shown in Figure 2. The visible absorption maximum of the dianion is at 490 nm. The monoanion has two visible maxima, one at 440 nm and the other at 470 nm (Figure 2A). The largest difference in the extinction coefficients of the mono- and dianion is at 420 nm. Moreover, the dianion extinction coefficient is very small at this wavelength. We recorded visible absorption spectra of fluorescein at five concentrations of *N*-AcAsp (0.005, 0.1, 0.4, 0.8, and 1 M) and different pH values in the range of 5.9−6.8. The observed effects of *N*-AcAsp concentration on the spectrum were very weak, and the isosbestic point was consistently around 460 nm.[31] These results indicate that the concentration of *N*-AcAsp has only small ionic strength effects on the ground-state equilibrium of these two prototropic forms of fluorescein. Hence, we conclude that *N*-AcAsp does not significantly perturb the absorption spectrum of the aqueous fluorescein solutions, and therefore, fluorescein does not form ground-state complexes with *N*-AcAsp.

Steady-State Emission Spectra. The emission spectrum of the monoanion shows a maximum at 510 nm and a shoulder around 550 nm. The emission spectrum of the dianion shows a maximum at 515 nm (Figure 2B). The emission efficiency is much greater for the dianion than monoanion. In Figure 3 the steady-state fluorescence spectra from aqueous fluorescein solutions in the presence of different concentrations of *N*-AcAsp, at pH 5.9, are shown. As can be seen, increasing the *N*-AcAsp concentration resulted in a pronounced increase in the intensities of the emission peak at 515 nm for $\lambda^{ex} = 440$ nm, and this effect saturated at 1 M *N*-AcAsp. At this pH the monoanion−dianion ratio in the ground state is > 1 and the 440 nm wavelength preferentially excites the less fluorescent monoanion (see Figure 2A). Because the 515 nm emission is dominated by dianion emission, these results indicate that increasing the *N*-AcAsp concentration increases the concentration of excited dianion molecules at pH 5.9. Thus, under these conditions, the excited monoanion is converted to the dianion during its lifetime. Similar results were obtained at the same excitation and emission wavelengths, but at the higher pH of 6.5.

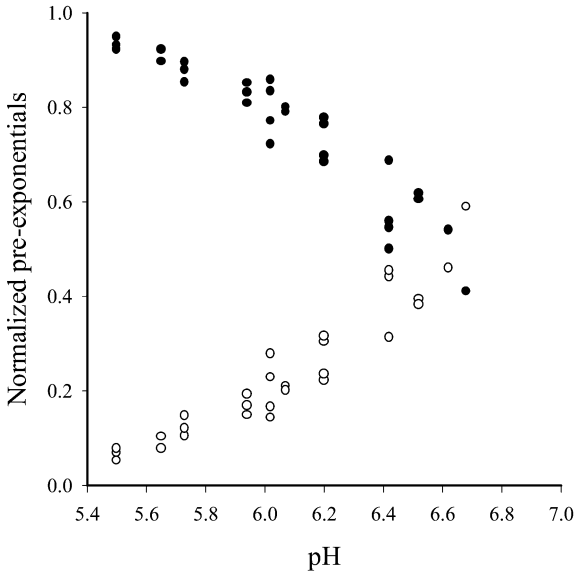

Figure 5. Plot of the normalized preexponential factors $\alpha_i/\sum_{j=1}^{2}\alpha_j$ vs pH. (●) corresponds to τ_1^0 and (○) corresponds to τ_2^0. The experimental values were obtained by global biexponential analysis of experimental decay traces from solutions of fluorescein and 5 mM *N*-AcAsp.

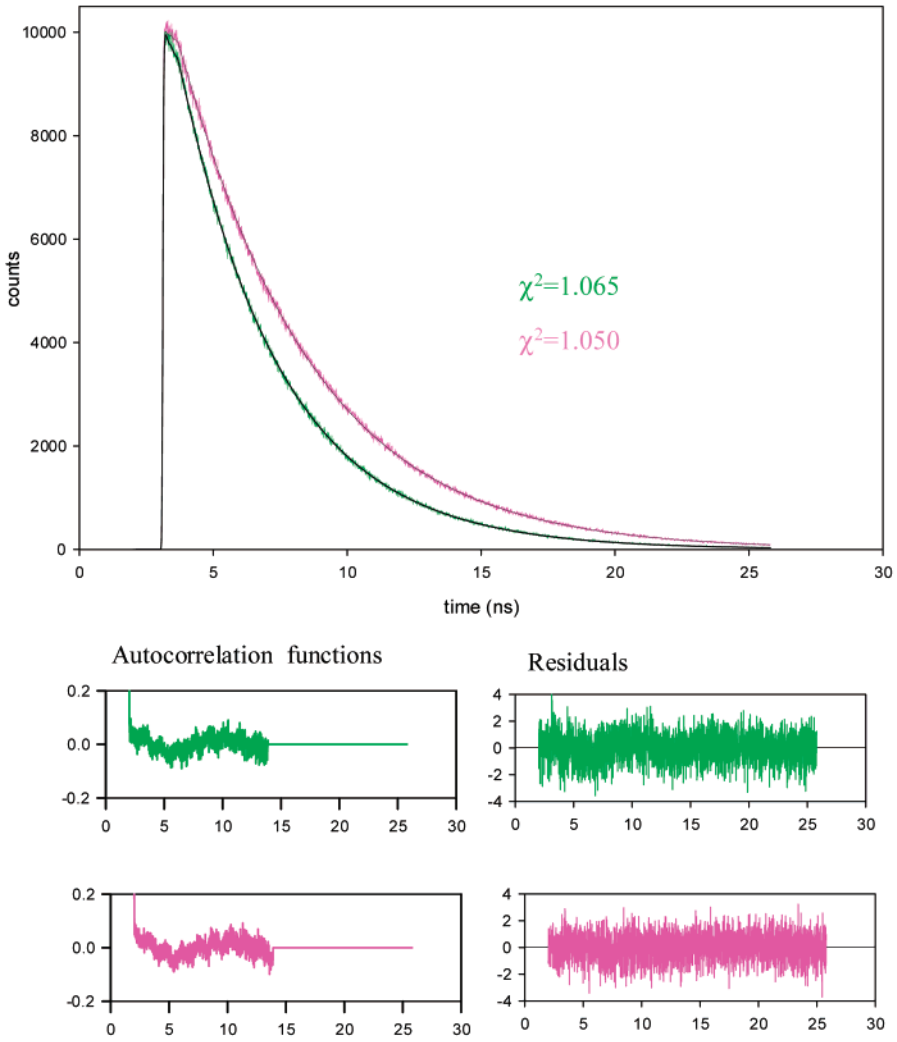

Figure 6. Experimental decay traces (green curve, 5 mM; magenta curve, 1 M), fitted functions (black curve), residuals, and autocorrelation functions of 2.5×10^{-5} M fluorescein in the presence of 5 mM *N*-AcAsp and 1 M *N*-AcAsp, pH 6.02, $\lambda^{ex} = 420$ nm, $\lambda^{em} = 515$ nm. For clarity reasons the instrument response functions are not displayed. The decays were extracted from two separate global biexponential analyses. The decay times and normalized preexponential coefficients recovered were $\tau_1 = 4.333$ ns, $\alpha_1 = 0.169$, $\tau_2 = 3.634$ ns, $\alpha_2 = 0.831$, for fluorescein in the presence of 5 mM *N*-AcAsp, and $\tau_1 = 4.325$ ns, $\alpha_1 = 0.599$, $\tau_2 = 3.217$ ns, $\alpha_2 = -0.401$, for fluorescein in the presence of 1 mM *N*-AcAsp. Note that the preexponential factor associated with the shorter lifetime at 1 M *N*-AcAsp concentration is negative.

As was demonstrated in a previous article, at pH values above 5, all excited cation and neutral fluorescein molecules rapidly convert with total efficiency to excited monoanions through excited-state proton transfer reactions.[3] Therefore, at pH values around 6, emission occurs only from the monoanion and dianion. Using these results and those from Figure 3, we assume a model in which the excited-state proton reactions of all the prototropic forms of fluorescein occur very rapidly during their excited-state lifetimes. Under these conditions the fluorescence intensity does not depend on which form is excited preferentially because the rapid proton transfer reaction in the excited-state erases all effects due to preferential excitation of any one form. For this model we can express the normalized fluorescence intensity by[3]

$$\frac{I}{A} = \frac{\phi_{F^-}}{1 + 10^{(pH - pK_a^*)}} + \frac{\phi_{F^{2-}}}{1 + 10^{(pK_a^* - pH)}} \qquad (17)$$

where I/A is the fluorescence intensity at λ^{em}, normalized by absorbance at the excitation wavelength, ϕ_{F^-} and $\phi_{F^{2-}}$ are the relative fluorescence efficiencies of the mono- and dianion at λ^{em}, and pK_a^* is the pK_a for the excited-state proton reaction $1^* \leftrightarrows 2^* + H^+$.

To quantify the reaction we have recorded titration graphs of fluorescence intensity, normalized by absorbance, versus pH for fluorescein solutions with *N*-AcAsp buffer concentration of 1 M at pH values between 5 and 10 ($\lambda^{ex} = 440$ nm; $\lambda^{em} = 515$ nm). This plot is shown in Figure 4. Equation 17 was fitted to the experimental results of Figure 4 by nonlinear least-squares estimation, and very good fit parameters were obtained ($r^2 = 0.998$), with a pK_a^* value of 6.59 ± 0.03. ϕ_{F^-} and $\phi_{F^{2-}}$ were floating values during the fitting. The $\phi_{F^-}/\phi_{F^{2-}}$ ratio obtained was 0.221 ± 0.004. Both pK_a^* and the $\phi_{F^-}/\phi_{F^{2-}}$ ratio were in accordance with those obtained in previous papers.[3,4] All these results, along with the good statistical parameters, show that the excited-state proton exchange reaction is sufficiently fast to occur during the excited lifetime.

Time-Resolved Emission. We recorded time-resolved emission traces with preferential monoanion (F^-) excitation at $\lambda^{ex} = 440$ nm (see Figure 2A) and preferential dianion (F^{2-*}) emission at $\lambda^{em} = 515$ nm (see Figure 2B), at low (5 mM) *N*-AcAsp concentration, in the pH range of 5.5−6.7. Our choices of excitation and emission wavelength allow the detection of the excited-state proton transfer reactions to be optimized. The lower pH range (<6.3) favors the monoanion F^-. It must be

emphasized that unambiguous detection of the excited-state proton transfer reaction would be possible when $\tilde{b}_1 = 1$ (only the monoanion F^- is excited) and $\tilde{c}_1 = 0$ (only the emission of the dianion F^{2-}* is recorded). In that case the decays would be dual exponential with a negative preexponential associated with the shorter decay time τ_S. At 5 mM *N*-AcAsp concentration the decays were biexponential with decay times independent of emission wavelength. The preexponential factors α were always positive, and the two lifetimes τ were pH independent. Because, in the absence of excited-state proton transfer reaction, fluorescein mono- (F^-*) and dianion (F^{2-}*) are not coupled and decay independently of each other, the recovered lifetimes actually correspond to those of the excited monoanion and dianion forms. The average of the experimental values of these lifetimes at different pH values and at 5 mM *N*-AcAsp were $\tau_S = 3.69 \pm 0.21$ ns and $\tau_L = 4.32 \pm 0.18$ ns. Moreover, above pH 8 the decays were monoexponential with τ around 4.3 ns. At pH values higher than pK_M (6.36), the monoanion concentration is insignificant, and therefore, the single lifetime displayed corresponds to the fluorescein dianion (F^{2-}*) lifetime ($\tau_2^0 = 1/k_{02}$ with $k_{02} = 2.31 \times 10^8$ s^{-1}). This value agrees with that obtained by other authors.[32,33] The smaller lifetime displayed in the pH range of 5.5−6.7 must therefore correspond to the fluorescein monoanion (F^-*) lifetime [$\tau_1^0 = 1/(k_{01} + k_{21})$ with $(k_{01} + k_{21}) = 2.71 \times 10^8$ s^{-1}]. The two values are in excellent agreement with those obtained at low phosphate buffer concentration (1 mM) in our previous article.[4]

Additional evidence for the assignment of the lifetimes $\tau_{1,2}$ to the excited states of fluorescein comes from the pH dependence of the preexponential factors $\alpha_{1,2}$. At pH values lower than pK_M (6.36) the monoanion (F^-) concentration is predominant; with increasing pH the dianion (F^{2-}) concentration increases. Because λ^{ex} and λ^{em} are fixed, the change in normalized preexponential factors will reflect the relative concentration change between F^- and F^{2-}. Higher pH values favor the dianion F^{2-}; as a consequence the normalized preexponential factor $\alpha_2/(\alpha_1 + \alpha_2)$ should increase. The lifetime τ_2 corresponding to this normalized $\alpha_2/(\alpha_1 + \alpha_2)$ is therefore associated with dianion (F^{2-}*). This is indeed experimentally observed (see Figure 5).

We also recorded fluorescence decay traces from solutions of 2.5×10^{-5} M fluorescein and 1 M *N*-AcAsp at different pH values in the range of 6.02 to 6.58. Time-resolved emission traces were recorded at two different excitation wavelengths, namely 420 and 440 nm, and emission was detected at 480, 500, 515, 530, 550, and 580 nm. Like the low *N*-AcAsp buffer case, the decay graphs were biexponential with decay times independent of emission wavelength. Nevertheless, contrary to the low *N*-AcAsp concentration case, the two lifetimes were pH dependent. The preexponential factors corresponding to the shorter lifetime were negative at emission wavelengths between 500 and 550 nm. These results support the hypothesis that there is a proton exchange between fluorescein and *N*-AcAsp in the excited state.

Figure 6 shows two illustrative decay traces extracted from two separate global biexponential analyses at 5 mM and 1 M *N*-AcAsp.

To estimate the preexponential factors $\alpha_{1,2}$ and lifetimes $\tau_{1,2}$ the experimental fluorescence decays recorded at various emission wavelengths at the same pH were analyzed globally as dual exponential functions (eq 9) with the lifetimes linked. The globally estimated lifetimes $\tau_{1,2}$ as a function of pH are shown in Figure 7. Finally, 28 decay traces were selected to be fitted by global compartmental analysis according to Scheme 2. The parameter linking scheme used is shown in Scheme 3. The rate constants k_{ij} are linked over the entire fluorescence decay surface; $\tilde{b}_1$ is linked at the same λ^{ex} and pH; $\tilde{c}_1$ is linked at the same λ^{em}. A series of global compartmental analyses was done in which the value of k_{02} was kept fixed at its true value ($k_{02} = 2.31 \times 10^8$ s^{-1}), while k_{01} was held constant at various values [$(0.0, 0.5, 1.0, 1.5, 2.0, 2.5, 2.71) \times 10^8$ s^{-1}]. The results of these global compartmental analyses are compiled in Table 1, and some illustrative examples are shown in Figure 8. The estimated values of k'_{12}, k'_{21}, $\tilde{b}_1$, and $\tilde{c}_1$ are independent of the (fixed) value of k_{01}. The estimated values of k_{21} vary as a function of k_{01} in such a way that the sum $(k_{01} + k_{21})$ is always constant at 2.765×10^8 s^{-1}. The contribution of the individual rate constants k_{01} and k_{21} to its sum cannot be determined from analyses as a function of pH at a single buffer concentration. The deterministic identifiability analysis (to be published separately) shows that at least two nonzero buffer concentrations and two pH values are necessary for the unique determination of all rate constants k_{ij}. Using the k_{ij} values of Table 1, the pK_{a2} value for *N*-AcAsp and the concentration of *N*-AcAsp used (1 M), we calculated $\tau_{1,2}$ according to eqs 10 and 11 at each pH. Figure 7 shows the plot of these $\tau_{1,2}$ values versus pH as lines. The points in Figure 7 are the $\tau_{1,2}$ values from the global biexponential analyses of the decay traces linked at each pH. The agreement between the two sets of lifetimes is excellent.

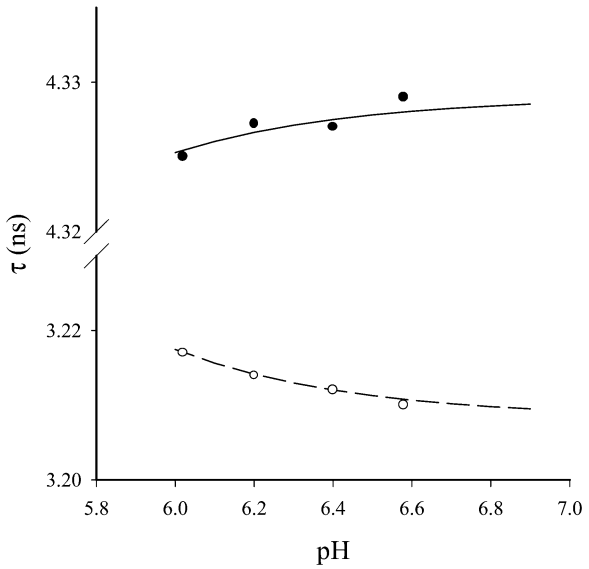

Figure 7. Graphs of $\tau_{1,2}$ vs pH for fluorescein in 1 M *N*-AcAsp buffered solutions. The symbols in this graph represent values obtained trough global biexponential analysis (eq 9) with $\tau_{1,2}$ linked at each pH. The solid and dashed lines are obtained with eqs 10 and 11 using the rate constants from Table 1 recovered by the single-step global compartmental analysis.

The pH dependence of $\tilde{b}_1(\lambda^{ex}, \text{pH})$ is exactly what is expected. Indeed, increasing the pH increases the dianion (F^{2-}) concentration, resulting in decreasing $\tilde{b}_1(\lambda^{ex}, \text{pH})$ values. Likewise the λ^{ex} dependence of $\tilde{b}_1(\lambda^{ex}, \text{pH})$ can be rationalized on the basis of absorption spectra (see Figure 2A). Indeed, the monoanion (F^-) absorbs relatively more than the dianion (F^{2-}) at $\lambda^{ex} =$ 420 nm compared to $\lambda^{ex} = 440$ nm.($\epsilon_{F^-}/\epsilon_{F^{2-}} = 4.23$ at $\lambda^{ex} =$ 420 nm and 2.52 at 440 nm). Bearing in mind that $\tilde{b}_1$ values are functions of ϵ_{F^-} and $\epsilon_{F^{2-}}$ at the excitation wavelength, as well as of the ground-state concentrations of monoanion and dianion, and these concentrations are, in turn, functions of pH

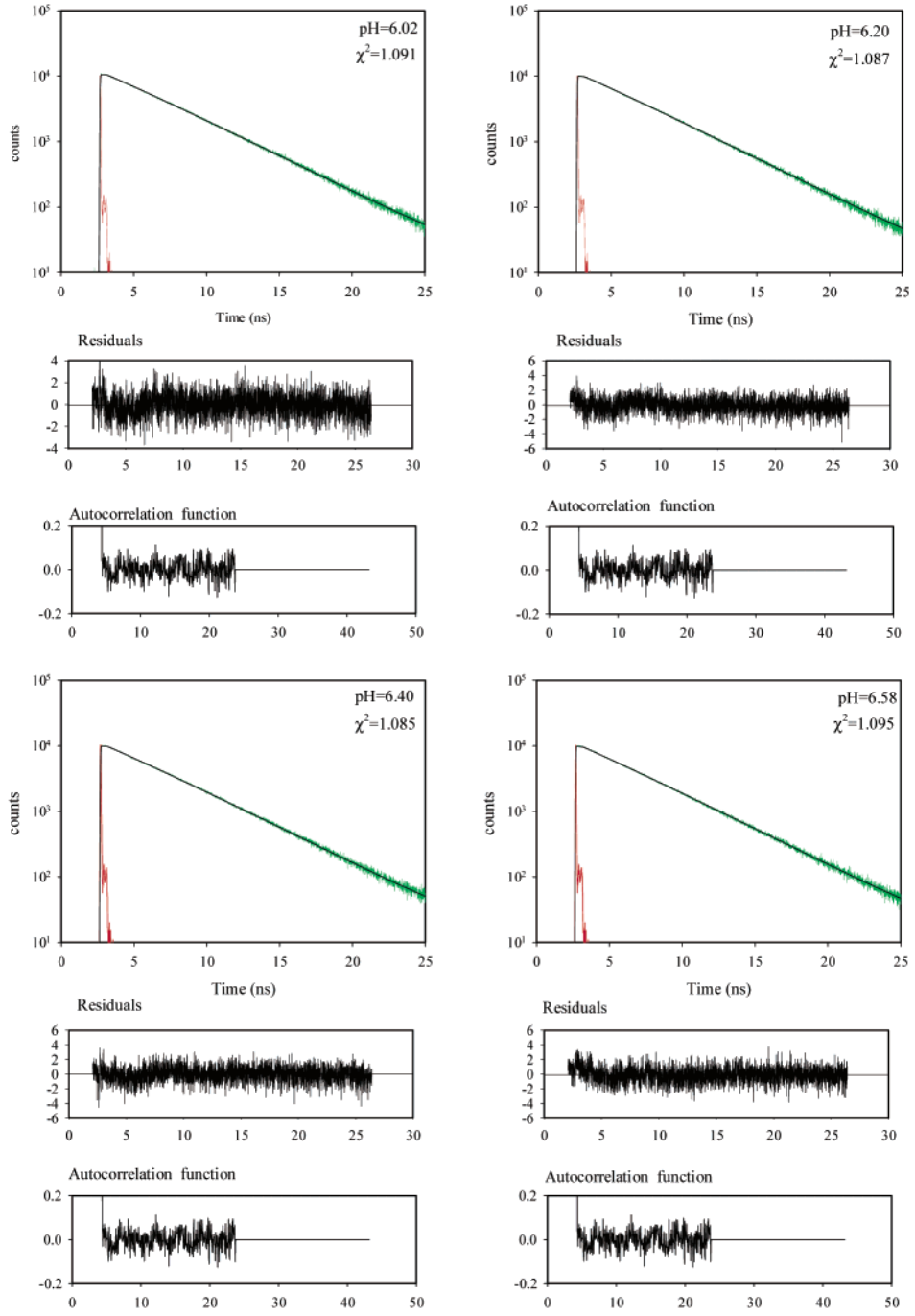

Figure 8. Plot of results obtained by means of global compartmental analysis of experimental decay traces of 2.5×10^{-5} M fluorescein and 1 M *N*-AcAsp at pH 6.02, 6.20, 6.40, and 6.58: (red curve) instrumental response function; (green curve) experimental decay at $\lambda^{ex} = 440$ nm and $\lambda^{em} = 515$ nm; (black curve) global compartmental fit. At the bottom of each curve are plotted the weighted residuals and the autocorrelation functions.

and the ground-state dissociation constant of fluorescein, we can define

$$\tilde{b}_1(\lambda^{ex}, \mathrm{pH}) = \frac{\frac{\epsilon_{F^-}}{\epsilon_{F^{2-}}}[H^+]}{\left(\frac{\epsilon_{F^-}}{\epsilon_{F^{2-}}}[H^+] + K_M\right)} \qquad (18)$$

Nonlinear least-squares fitting of eq 18 to the $\tilde{b}_1$ data of Table 1 results in $\epsilon_{F^-}/\epsilon_{F^{2-}}$ values of 5.35 (λ^{420}) and 4.57 (λ^{440}), which agree with those obtained in our previous paper (5.99 and 3.98, respectively),[4] although they are somewhat higher than those calculated from absorption data. The dependence of $\tilde{c}_1(\lambda^{em})$ on λ^{em} can be rationalized on the basis of the fluorescence spectra of Figure 2B. At longer wavelengths relatively more emission originates from the monoanion (F^{-*}), resulting in higher $\tilde{c}_1(\lambda^{em})$ values.

Conclusions

We have presented absorption, steady-state emission, and fluorescence decay traces for fluorescein in solutions at low and high *N*-AcAsp concentrations and different pH values. The results clearly show an excited-state proton transfer reaction between the mono- and dianion of the fluorescein in the presence of *N*-AcAsp, and this reaction is sufficiently fast to occur during the excited lifetime of the fluorescein when the *N*-AcAsp

concentration is high (1 M). For this fluorescein monoanion−dianion excited-state proton reaction we have evaluated the kinetic and spectral parameters. To determine these fundamental parameters, a multidimensional fluorescence decay data surface was measured at different pH values and various excitation and emission wavelengths. The accurate determination of the decay times and the preexponentials was done by global biexponential analysis in which the lifetimes were linked at each pH. The entire fluorescence decay surface at different pH values, λ^{ex}, and λ^{em} was analyzed by global compartmental analysis according to Scheme 2 with the parameters linked as shown in Scheme 3. This analysis method has the additional advantage that the parameters of interest were determined directly from the complete decay data surface in a single step.

The kinetics model and method of analysis which we have presented are applicable to any two-state excited-state reaction in the presence of buffer. This powerful analysis tool can be used to reveal how the complex behavior of fluorescein-labeled proteins is influenced by amino acid side chains.

Acknowledgment. J.T. thanks the I. W. T. for a doctoral fellowship. M.C. is a postdoctoral fellow at the K. U. Leuven. L.C. thanks the Spanish Ministry of Science and Technology for a Ph.D. fellowship and a travel grant to the K. U. Leuven. He also thanks the K. U. Leuven for the hospitality shown him during his stay. N.B. is grateful to the Universidad de Granada for a grant allowing him to stay there. This work was supported by Grants PB98-1285 and BQU2002-01311 from the Spanish Ministry of Science and Technology. The Fonds voor Wetenschappelijk Onderzoek Vlaanderen and DWTC (Belgium) through IAP-V-03 are thanked for continuing support to the K. U. Leuven research group.

References and Notes

(1) Zanker, V.; Peter, W. *Chem. Ber.* **1958**, *91*, 572−580.
(2) Diehl, H.; Horchak-Morris, N. *Talanta* **1987**, *34*, 739−741.
(3) Yguerabide, J.; Talavera, E.; Alvarez, J. M.; Quintero, B. *Photochem. Photobiol.* **1994**, *60*, 435−441.
(4) Alvarez-Pez, J. M.; Ballesteros, L.; Talavera, E. M.; Yguerabide, J. *J. Phys. Chem. A* **2001**, *105*, 6320−6332.
(5) Costa Pesoa, J.; Gadja, T.; Gillard, R.; Kiss, T.; Luz, S. M.; Moura, J. J. G.; Tomaz, I.; Telo, J. P.; Török, I. *J. Chem. Soc., Dalton Trans*. **1998**, 3587−3600.
(6) Wilson, N. A.; Barbar, E.; Fuchs, J. A.; Woodward, C. *Biochemistry* **1995**, *34*, 8931−8939.
(7) Tissot, A. C.; Vuilleumier, S.; Fersht, A. R. *Biochemistry* **1996**, *35*, 6786−6794.
(8) Oliveberg, M.; Fersht, A. R. *Biochemistry* **1996**, *35*, 6795−6805.
(9) Rozwadowski, M. *Acta Phys. Pol.* **1961**, *20*, 1005−1017.
(10) Knutson, J. R.; Beechem, J. M.; Brand, L. *Chem. Phys. Lett.* **1983**, *102*, 501−507.
(11) Beechem, J. M.; Brand, L. *Photochem. Photobiol.* **1986**, *44*, 323−329.
(12) Janssens, L. D.; Boens, N.; Ameloot, M.; De Schryver, F. C. *J. Phys. Chem.* **1990**, *94*, 3564−3576.
(13) Beechem, J. M.; Ameloot, M.; Brand, L. *Chem. Phys. Lett.* **1985**, *120*, 466−472.
(14) Ameloot, M.; Beechem, J. M.; Brand, L. *Chem. Phys. Lett.* **1986**, *129*, 211−219.
(15) Ameloot, M.; Boens, N.; Andriessen, R.; Van den Bergh, V.; De Schryver, F. C. *J. Phys. Chem.* **1991**, *95*, 2041−2047.
(16) Andriessen, R.; Boens, N.; Ameloot, M.; De Schryver, F. C. *J. Phys. Chem.* **1991**, *95*, 2047−2058.
(17) Jacquez, J. A. *Compartmental Analysis in Biology and Medicine*; Elsevier: Amsterdam, 1972.
(18) Godfrey, K. *Compartmental Models and Their Application*; Academic Press: London, 1983.
(19) Anderson, D. H. *Compartmental Modeling and Tracer Kinetics*; Lecture Notes in Biomathematics, Vol. 50; Springer-Verlag: Berlin, 1983.
(20) Beechem, J. M.; Ameloot, M.; Brand, L. *Anal. Instrum.* **1985**, *14*, 379−402.
(21) Khalil, M. M. H.; Boens, N.; Van der Auweraer, M.; Ameloot, M.; Andriessen, R.; Hofkens, J.; De Schryver, F. C. *J. Phys. Chem.* **1991**, *95*, 9375−9381.
(22) Van den Bergh, V.; Boens, N.; De Schryver, F. C.; Ameloot, M.; Gallay, J.; Kowalczyk, A. *Chem. Phys.* **1992**, *166*, 249−258.
(23) Meuwis, K.; Depuydt, G.; Boens, N.; De Schryver, F. C. *Chem. Phys. Lett.* **1995**, *246*, 641−648.
(24) Boens, N.; Kowalczyk, A.; Cielen, E. *J. Phys. Chem.* **1996**, *100*, 4879−4887.
(25) Boens, N.; Szubiakowski, J.; Novikov, E.; Ameloot, M. *J. Chem. Phys.* **2000**, *112*, 8260−8266.
(26) Leonhardt, H.; Gordon, L.; Livingston, R. *J. Phys. Chem.* **1971**, *75*, 245−249.
(27) Maus, M.; Rousseau, E.; Cotlet, M.; Schweitzer, G.; Hofkens, J.; Van der Auweraer, M.; De Schryver, F. C. *Rev. Sci. Instrum.* **2001**, *72*, 36−40.
(28) Program developed jointly by the Technology Institute of the Belarusian State University (Minsk, Belarus) and the Division of Photochemistry and Spectroscopy of the K. U. Leuven (Leuven, Belgium).
(29) Smith B. T.; Boyle J. M.; Garbow B. S.; Ikeke Y.; Klema V. C.; Moler C. B. In *Lecture Notes in Computer Science*; Goos, G., Hartmanis, J., Eds.; Springer-Verlag: Heidelberg, New York, 1974; Vol. 6.
(30) Diehl, H. *Talanta* **1989**, *36*, 413−415.
(31) Crovetto, L. Ph.D. Thesis, University of Granada, Granada, Spain, 2003.
(32) Flamigni, L. *J. Phys. Chem.* **1993**, *97*, 9566−9572.
(33) Sjöback, R.; Nygren, J.; Kubista, M. *Spectrochim. Acta, Part A* **1995**, *51*, L7−L21.